ANTIOXIDANTS & REDOX SIGNALING
Volume 11, Number 1, 2009

DOI: 10.1089/ars.2008.2068

Original Research Communication

Identification, Expression Pattern, and Characterization of Mouse Glutaredoxin 2 Isoforms

Christoph Hudemann,[1] Maria Elisabet Lönn,[1] José Rodrigo Godoy,[2] Farnaz Zahedi Avval,[1] Francisco Capani,[3] Arne Holmgren,[1] and Christopher Horst Lillig[1,2]

Abstract

Glutaredoxin 2 (Grx2) is a glutathione-dependent oxidoreductase involved in the maintenance of mitochondrial redox homeostasis. Grx2 was first characterized as mitochondrial protein, but alternative mRNA variants lacking the transit peptide-encoding first exon were demonstrated for human and proposed for mouse. We systematically screened for alternative transcript variants of mouse Grx2. We identified a total of six exons, three constitutive (II, III, and IV), two alternative first exons (exons Ia and Ic), and one single-cassette exon (exon IIIb) located between exons III and IV. Exons Ic and IIIb are not present in the human genome; mice lack human exon Ib. The six exons give rise to five transcript variants that encode three protein isoforms: mitochondrial Grx2a, a cytosolic isoform that is homologous to the cytosolic/nuclear human Grx2c and present in specific cells of many tissues and the testis-specific isoform Grx2d that is unique to mice. Mouse Grx2c can form an iron/sulfur cluster–bridged dimer, is enzymatically active as a monomer, and can donate electrons to ribonucleotide reductase. Testicular cells lack mitochondrial Grx2a but contain cytosolic Grx2. Prominent immunostaining was detected in spermatogonia and spermatids. These results provide evidence for additional functions of Grx2 in the cytosol, in cell proliferation, and in cellular differentiation. *Antioxid. Redox Signal*. 11, 1–14.

Introduction

Glutaredoxin (Grx) is a small ubiquitous protein that is involved in the maintenance of cellular redox homeostasis. It was first discovered as a hydrogen donor for ribonucleotide reductase (RNR) in *Escherichia coli* (12) but has since been identified in a wide range of organisms, including eukaryotes, prokaryotes, and viruses. Grx effectively catalyzes the reduction of both glutathione-mixed disulfides and protein disulfides by using one or two redox-active cysteines in its active site, respectively [for an overview, see (4) and (19)]. This active-site motif, Cys-*X*-*X*-Cys, is characteristic among a growing number of redox active enzymes that constitute the thioredoxin family of proteins. Thioredoxins (Trxs) and Grxs share a similar three-dimensional structure called the thioredoxin fold (28) and reduce disulfides with electrons provided from NADPH *via* thioredoxin reductase (TrxR) and glutathione/glutathione reductase, respectively (13). Complete Trx and Grx systems are present in both cytosol and mitochondria (8, 24, 30). Three different mammalian Trx systems have been described: the cytosolic Trx1/TrxR1, the mitochondrial Trx2/TrxR2, and thioredoxin and glutathione reductase (TGR). TGR differs from the two other TrxRs because of an N-terminal Grx domain. It is expressed predominantly in testis, has a broad substrate specificity, and can reduce components from both the Trx and Grx systems (45, 46).

At present, two different Grxs have been characterized in mammals. Cytosolic Grx1 contains the active-site sequence Cys-Pro-Tyr-Cys and is involved in various redox-depen-

[1]Medical Nobel Institute for Biochemistry, Department of Medical Biochemistry and Biophysics, Karolinska Institutet, Stockholm, Sweden.
[2]The Institute for Clinical Cytobiology and Cytopathology, Phillips Universität, Marburg, Germany.
[3]The Department of Biochemistry, School of Medicine, University of Buenos Aires, Buenos Aires, Argentina.

dent cellular processes, such as reduction of ribonucleotides and dehydroascorbate (12, 50), actin polymerization (49), and protection against oxidative stress and apoptosis (5, 32); for a detailed overview, see (4, 19, 43)]. The second mammalian Grx (Grx2), localized predominantly in mitochondria, was identified more recently (8, 24). The protein levels of total Grx2 are significantly lower compared with the levels of Grx1 in placenta and cell lysates from various tumor cell lines (23). It was suggested that Grx2 plays a central role in the interplay between GSH and the thiol groups of mitochondrial membrane proteins (2). Transient silencing of Grx2 expression in HeLa dramatically sensitized these adenocarcinoma cells to apoptosis induced by phenylarsine oxide and the anticancer agent doxorubicin (21). Overexpression of Grx2 attenuates apoptosis induced by doxorubicin and the antimetabolite 2-deoxy-D-glucose by sustaining mitochondrial redox homeostasis, thereby preventing cardiolipin oxidation, cytochrome c release, caspase activation, and ultimately, cell death (7).

The active-site sequence of Grx2 (Cys-Ser-Tyr-Cys) differs from the Grx consensus sequence, with the Pro being exchanged for Ser. This exchange has two remarkable consequences. First, Grx2 can be reduced not only by GSH, but also by thioredoxin reductase (16). The physiologic importance of this reaction remains to be established; however, this electron pathway might play a role under conditions in which the GSH/GSSG ratio decreases or the cellular pH decreases or both. Second, it allows the protein to complex a 2Fe2S cluster (3, 20). This cluster bridges two Grx2 monomers to form a dimeric holo-Grx2 complex. The chromophore is complexed by the two N-terminal active-site thiols of the proteins and the thiol groups of two molecules of GSH non-covalently bound to the Grx2 monomers (3, 15). The holo-complex lacks enzymatic activity; dissociation of the cluster yields active monomeric apoprotein. Oxygen-dependent degradation of the holo-complex is efficiently prevented by reduced GSH. GSSG and other redox-active compounds conversely promote degradation (20).

The human Grx2 gene (GLRX2) is located at chromosome 1q31.2-31.3 (24) and gives rise to three alternatively transcribed Grx2 mRNA isoforms with alternative first exons (22, 24). These mRNA variants encode three distinct proteins: (a) the ubiquitous Grx2a (exons Ia–IV) that is targeted to mitochondria; (b) Grx2b (exons Ib–IV); and (c) Grx2c (exons $Ib^{truncated}$–IV) share a cytosolic and nuclear localization pattern. Their expression is restricted to testis and cancer cells (22). In mouse, mRNA variants of Grx2 differing in the 5′ end have been proposed (8). One of these variants contains a mitochondrial signal peptide and corresponds to the human mitochondrial isoform, Grx2a. However, no counterpart for the proposed alternative exon Ib, which gives rise to the cytosolic/nuclear isoforms Grx2b and Grx2c, is present in the mouse gene. Analyzing the absolute gene-expression pattern of Grx2 in mouse, Jurado *et al*.(17) found that Grx2a mRNA accounted for only 40% of the total amount of Grx2 mRNA in most organs. The remarkable exception to this were testes, in which only 1% of the total Grx2 mRNA accounted for the Grx2a variant. These studies strongly indicated the presence of further Grx2 transcript variants in mouse as well. Here, we present the identification of these additional transcript variants, their expression pattern in multiple tissues, and a characterization of a new nonmitochondrial Grx2 protein isoform that is present in many tissues.

Material and Methods

Materials and general methods

Chemicals and enzymes were purchased from Sigma, unless otherwise stated, and were of analytic grade or better. C57BL/6J mice were purchased from the Jackson Laboratory (Bar Harbor, ME). All experiments involving animals were approved by the respective authorities. SDS-PAGE was run by using the Novex Mini-Cell and precast NuPAGE gels (12% acrylamide, Bis-Tris, Invitrogen, Carlsbad, CA) according to the manufacturer's instructions.

Analysis of EST sequences

Based on the sequences of the proposed mouse glutaredoxin 2 exons Ia, II, III, and IV (*e.g.*, GeneBank accession number AF380337), an extensive EST cluster search was carried out. Each exon was compared with the GenBank mouse EST database by using the BlastN algorithms (1). Sequences with down to 40-bp matches were analyzed in detail. When necessary, sequences were reoriented, and each EST sequence was individually mapped to the genomic sequence (AL592403) by using EST2genome from the EMBOSS package (http://emboss.sourceforge.net) to identify potential exon–intron boundaries.

cDNA and PCR

For the identification of transcript variants and analysis of expression patterns, multiple tissue cDNA panels I and II (Clontech, Mountain View, CA) were purchased, which included primers for the amplification of glyceraldehyde-3-phosphate dehydrogenase (G3PDH), which served as positive control. Additional cDNA was produced from C57BL/6J mice. RNA isolation was done by using RNeasy Mini Kit (Qiagen, Hilden, Germany) followed by immediate first-strand cDNA synthesis by using the Omniscript RT-Kit (MBI Fermentas, St. Leon-Rot, Germany) as suggested by the manufacturer by using an oligo-dT primer and 3 μg of RNA. Oligonucleotides for PCR (summarized in Table 1) were ordered from DNA technology (Aarhus, Denmark). Reactions were performed in programmable thermocyclers from MJ Research in a total volume of 20 μl containing 1.25 U recombinant Taq polymerase, 200 μM dNTPs, 1.5 mM Mg^{2+} (all MBI Fermentas), 0.5 m*M* of each primer, and ~4 ng first-strand cDNA. After an initial denaturation step at 95°C for 2 min, 35 cycles of the following program were performed: 95°C for 30 sec, reaction-specific annealing temperatures (see Table 1) for 45 sec, and 72°C for 40 sec. The final elongation step was performed at 72°C for another 10 min. For transcript variant mGLRX_v2, we used EST-clone P998004867 from the I.M.A.G.E. Consortium as positive control. In general, PCR products were analyzed on 1.5% agarose gels (14.5 × 19 cm containing 40 m*M* Tris, 19 m*M* acetic acid, and 1 m*M* EDTA). Selected PCR fragments were extracted from agarose gels by using the Qiagen Gel Extraction Kit and directly ligated into pGEM-T vector (Promega, Madison, WI). The plasmids were subsequently sequenced from both 3′ and 5′ directions by the core facility of the Karolinska Institute, KISeq. The densiometric analysis of band intensities was performed by using the Kodak 1D software, version 3.5.

Table 1. Oligonucleotides and Polymerase Chain Reactions

Oligonucleotides

Name	*Target exon*	*Size*	*Sequence*
PR89	Ia	25	5′-GCTGGTGGCGAGCGGGAGGATCTTG-3′
PR108	Ia/Ia^{trunk}	18	5′-CTGCTCTCCCGGAGGCTG-3′
PR119	Ic/Ic^{trunk}	29	5′-CTTAAGATGACATTCCGGTCCGGTCCATC-3′
PR90	Id	28	5′-GTGCCTGCCCCTTTCCTTAATAGGAAAG-3′
PR91	II	30	5′-CAGCACATCGTCGTTTTGGGGGAAGTCTAC-3′
PRCH6	IIIb (reverse)	27	5′-TCAGGCAACTACTGAGATTTTTTTCAG-3′
PR105	IIIb	27	5′-CTCAGTAGTTGCCTGAGGGAGAGAATG-3′
PR93	IV (reverse)	27	5′-CACTGATGAACCAGAGGCAGCAATTTC-3′
PR94	IV-UTR (reverse)	28	5′-CAGCCTCAAGTCAAAGGTACGACTGCAC-3′

Polymerase chain reactions

Oligonucleotides	*Target sequence*	*Expected length*	*Annealing temperature*	*Positive control*
G3PDH Primermix	G3PDH for each tissue	983	55	Pooled cDNA
PR91/PR94	Exon II-IV UTR rev	430	58	Pooled cDNA
PR89/PR94	Exon Ia-IV UTR rev	502	58	Pooled cDNA
PR119/PR94	Exon Ic/Ic^{trunc}-IV UTR rev	658/526	56	Pooled cDNA
PR90/PR94	Exon Id-IV UTR rev	502	54	None available
PR108/PR93	Exon Ia/Ia^{trunc}-IV rev	471/397	54	EST clone P998004867
PR108/PRCH6	Exon Ia/Ia^{trunc}-IIIb rev	365	54	None available
PR105/PR94	Exon IIIb-IV UTR rev	269	55	None available

Rapid amplification of cDNA ends (5′ RACE)

To obtain the 5′ end of the newly identified Grx2 mRNA variants, the GeneRacer kit (Invitrogen) was used, according to the manufacturer's recommendations. In brief, 2.5 μg total RNA from mouse testis were dephosphorylated and decapped. The RNA Oligo was ligated to the 5′ end of the mRNA and subsequently reverse transcribed with the GeneRacer Oligo dT Primer by using SuperScript III Reverse Transcriptase (Invitrogen). 5′-RACE reactions were performed by using the gene specific primer 5′-cac tga tga acc aga ggc agc aat ttc-3′ and the GeneRacer 5′ Primer. For each reaction, 2 μl of cDNA and 0.5 μl of DyNAzyme EXT DNA polymerase (Finnzymes) were used to amplify the fragment by touchdown PCR method by using the following conditions: One cycle at 94°C, 2 min; 10 cycles at 94°C, 15 sec; 76°C, 30 sec, minus 0.5°C each cycle, and 72°C, 1 min; Thirty cycles at 94°C, 15 sec; 71°C, 30 sec; and 72°C, 1 min plus 5 sec for each cycle; and final extension at 72°C for 7 min. After amplification, samples were kept at 4°C until analysis. The 5′-RACE fragment was gel-purified and cloned into pCR4-TOPO vector (Invitrogen). Positive clones were analyzed by PCR and sequencing.

Cloning, recombinant expression, and purification of mouse Grx2 isoforms

The open reading frames of mouse Grx2c and Grx2d were amplified from pooled cDNA by using the following oligonucleotides: 5′ for both reactions: CACACACATATGGGAAACAGCACATCGTCG, 3′ reverse for Grx2c: CACACAGGATCCTCAATGTCTTTCCTCTTGTTTTTTTTTTAAATAACAC, and 3′ reverse for Grx2d: CACACAGGATCCTCAGGCAACTACTGAGATTTTTTTCAG. The PCR products were ligated into the NdeI and BamH1 sites of pET15b (Novagen, Darmstadt, Germany). Human Grx2c and mouse Grx2c were essentially expressed and purified as described earlier (20), replacing nickel nitrilotriacetic acid columns with Talon columns (Clontech) of 5 ml. Bound protein was eluted with a 200-ml linear gradient of imidazole from 0 to 300 m*M* in 50 m*M* sodium phosphate, pH 8, containing 300 m*M* NaCl. Preparation of apo Grx2c was done with high-performance liquid chromatography, as described in reference (20).

Grx2d was not expressed in soluble form. Therefore, we used a modified protocol for *in vitro* folding of inclusion body proteins (38). As described earlier, cells were disrupted by a combination of lysozyme treatment and sonication. The crude extract was centrifuged at 20,000 g for 30 min. The pellet containing Grx2d inclusion bodies was resuspended in 50 m*M* sodium phosphate buffer, pH 8, 300 m*M* NaCl, and 1% Triton-X100 and centrifuged at 12,000 *g* for 30 min. The pellet was resuspended in 50 m*M* sodium phosphate buffer, pH 8, containing 300 m*M* NaCl, and centrifuged in the same way. Next, the pellet was resuspended in 6 *M* guanidine HCl, 100 m*M* dithiotreitol, and 100 m*M* Tris/HCl, pH 8, and incubated for 2 h at room temperature with gentle shaking. The protein solution was centrifuged at 20,000 *g* for 30 min. The supernatant was collected, and dithiothreitol was removed by using prepacked Sephadex G-25 gel filtration columns (PD10, Amersham, Uppsala, Sweden) equilibrated with 6 *M* guanidine HCl and 100 m*M* Tris/HCl, pH 8. The protein was purified by immobilized metal-affinity chromatography by using a Talon column of 3 ml. Unspecific bound protein was removed by two wash steps with 50 m*M* sodium phosphate, pH 8, 300 m*M* NaCl, 6 *M* guanidine HCl, and the same buffer containing 50 m*M* imidazole. The protein was eluted in the washing buffer containing 300 m*M*

imidazole. The pure protein was stepwise diluted 12-fold with 50 m*M* sodium phosphate, pH 8, 500 m*M* NaCl containing 50% glycerol over a period of 4 h on ice to allow gentle refolding of the protein. Residual guanidine and imidazole were removed by using PD10 columns equilibrated with the dilution buffer.

Protein concentrations were determined spectrophotometrically by using the absorbance coefficients of 11,460 M/cm for Grx2c and 9,870 M/cm for Grx2d at 280 nm. These absorbance coefficients were calculated from the protein sequences by using ProtParam (www.expasy.ch).

ELISA

Organ tissue from two different mice (except for liver, for which only one organ was used) were homogenized in 400 μl lysis buffer (10 m*M* Tris/HCl, pH 7.4, 10 m*M* NaCl, 3 m*M* $MgCl_2$, 0.1 % Nonidet P40) by using pellet pestles (Kontes Glass Company, Vineland, NJ) in an Eppendorf tube. After 15 min at room temperature, the samples were frozen in liquid nitrogen. After thawing, the samples were centrifuged at 20,000 *g* for 60 min at 4°C. The total protein concentration in the supernatant was determined by using Bradford Reagent (BioRad, Hercules, CA) with a BSA-standard from 0.01 to 0.8 mg/ml. Quantification of mouse Grx2 was done by using a specific sandwich ELISA, as described by Lundberg*et al*. (23). The antibody used in this ELISA was raised against recombinant human Grx2c and thus recognizes all isoforms. Human Grx2c was exchanged for mouse Grx2c to generate the standard curve used for quantification.

Immunohistochemistry and immunofluorescence

Mouse testes were dissected and fixed for 24 h in either Carnoy (immunofluorescence) or 3.7% formalin (immunohistochemistry). After dehydration, the testes were processed for paraffin embedding. Sections (10 μm thick) were cut and placed on poly-L-lysine–coated slides. The sections were deparaffinized and incubated in 3% hydrogen peroxide for 30 min to quench endogenous peroxidase. After three washes in PBS, nonspecific antibody-binding sites were blocked with 5% normal goat serum (Invitrogen). Next, sections were incubated overnight with the primary antibody, rabbit anti-mouse Grx2 (diluted 1:1,000), at 4°C. The mouse Grx2 antibody was generated as described by Lundberg *et al*. (24) by using recombinant mGrx2c and detects Grx2a, processed Grx2a, and Grx2c. Negative controls were incubated with goat serum in PBS. The following day, sections were washed with PBS and subsequently incubated with a biotinylated goat anti-rabbit antibody diluted 1:500 (Invitrogen, Karlsruhe, Germany) for 30 min at room temperature. For immunohistochemistry, the StreptABComplex/HRP (Dako Cytomation, Hamburg, Germany) was used for antigen staining, according to the manufacturer's recommendations. The sections were incubated with the substrate aminoethyl carbazole (AEC; Invitrogen, Karlsruhe, Germany) for 5 min at room temperature, counterstained with Mayer's hematoxylin, and mounted with Mowiol. For immunofluorescence studies, the TSA kit (Tyramide Signal Amplification; Invitrogen) was used. In brief, after incubation with the biotinylated secondary antibody, the sections were incubated with a streptavidin-conjugated horseradish peroxidase for 30 min at room temperature. After three PBS washing steps, sections were incubated with the Alexa Fluor 488–labeled tyramide for 5 min at room temperature. Sections were counterstained with Hoechst 33342 (Sigma).

The cellular localization of Grx2 in mouse tissues was analyzed by fluorescent co-staining with cytoplasmatic (DNase I, Invitrogen) and mitochondrial markers (anti-prohibitin 1, Calbiochem or anti-manganese superoxide dismutase (MnSOD, Alexis). Instead of the signal-amplification kit described earlier, an antigen-recovery step was introduced by heating the slides in citrate buffer (10 m*M*, pH 6.0) for 14 min in a microwave oven. After incubation overnight with the anti-mouse Grx2 (1:200) and the anti-prohibitin 1 (1:200) or anti-MnSOD (1:200) antibodies, the slides were developed with goat anti-rabbit Alexa Fluor 633 (1:300), detecting anti-Grx2, and chicken anti-mouse Alexa 488 (1:500, both Invitrogen), detecting anti-prohibitin 1 or anti-MnSOD. Alexa Fluor 488–labeled DNase I was applied at 9 μg/ml for 20 min for the labeling of globular actin. DNA was counterstained with Hoechst as described earlier; the slides were mounted with Mowiol.

Sections prepared for immunohistochemistry were examined with a Leica Diaplan microscope equipped with a MicroPublisher camera (QImaging, Surrey, BC, Canada). Samples prepared for immunofluorescence were analyzed with a Leica TCS SP2 confocal laser scanning microscope by using a 40× oil planapochromatic lens (Leica, Heidelberg, Germany). Deconvolution and 3D reconstruction was performed by using the software package Huygens (Scientific Volume Imaging, Hilversum, The Netherlands).

Analysis of chromophore and quaternary structure

UV-visible spectra were recorded with a Shimadzu UV-2100 spectrophotometer. The presence of dimeric Grx2c and the molecular weights were confirmed with high-performance liquid chromatography (Amersham Smart system) by using a Superdex 75 3.2/30 precision column equilibrated with 50 m*M* sodium phosphate, pH 8, and 300 m*M* NaCl, as described in (20). The Low Molecular Weight Gel Filtration Calibration Kit (Amersham) was used for calibration.

Enzymatic assay

Grx2 activity was measured by using a modified protocol of the hydroxyethyl disulfide (HED)-assay (25) in a total volume of 200 μl. In brief, 50 μl HED (0.7 m*M* final concentration) was added to 100 Êl of a freshly prepared substrate mix containing 100 m*M* Tris/HCl, pH 8.0, 2 m*M* EDTA, 0.1 mg/ml BSA, 1 m*M* GSH, 240 μM NADPH, and 6 μg/ml yeast glutathione-reductase (final concentrations). After 4 min of preincubation at 30°C, different amounts of Grx in a volume of 50 μl (0,10, 25, 50, 75, 100, 150, and 200 nM final concentration, respectively) were added. The decrease in absorbance at 340 nm was measured at 30°C in a 96-well plate by using a VERSAmax microplate reader (Molecular Devices). NADPH consumption was quantified based on 12 standards of NADPH from 0 to 240 μM concentration. Activity was expressed as micromoles of NADPH oxidized per min.

RNR activity was determined by following the conversion of [^{3}H]CDP into [^{3}H]dCDP with mouse RNR, according to the methods of Thelander and co-workers (6, 27). Reducing equivalents for Grx2c were provided through 4 m*M* GSH, glutathione reductase, and NADPH (25). The reaction was

initiated by adding mouse RNR (5.5 μg of R1 and 2.1 μg of R2) to the reaction mixture containing 40 m*M* Tris-Cl buffer, pH 7.5, 2 m*M* ATP, 10 m*M* magnesium chloride, 200 m*M* potassium chloride, and 0.5 m*M* [^{3}H]CDP (23,000 cpm/nmol) in a final volume of 50 μl. Samples were incubated at 37°C, and the reaction was terminated after 30 min by the addition of 1 *M* $HClO_4$ followed by acid hydrolysis. The amount of [^{3}H]dCDP formed was calculated from the results of liquid scintillation counting after ion-exchange chromatography separation of the monophosphates on Dowex-50 columns.

Nomenclature

We have used the official Grx2 gene name GLRX2 when discussing properties of the gene. Transcript variants were named as proposed by the International Committee on Standardized Genetic Nomenclature for Mice (http://www.informatics.jax.org/mgihome/nomen/gene.shtml). The commonly used abbreviation Grx was used to describe the proteins. To avoid any possibility of confusion, we have kept and extended the nomenclature for Grx2 exons and isoforms introduced by Lundberg*et al*. (24). The newly identified alternative first exon was named exon Ic to avoid confusion with human exon Ib, not present in mouse. The new protein variants were named Grx2c and Grx2d.

Results

Identification and expression pattern of Grx2 transcript variants

The gene encoding mouse Grx2 (GLRX2) is located on chromosome 1 (1 77.8 cM) and consists of four exons spanning ~12 kb. We systematically screened the mouse genome database for EST sequences homologous to at least one of the Grx2 proposed exons (8) and identified >100 unique entries. We aligned these potential mRNA variants pairwise to the genomic sequence, analyzed the genomic structure, and identified a variety of potential exons and splice variants. To verify the additional exons and variants and to analyze the expression pattern of Grx2 transcript variants, we screened mouse cDNA derived from heart, brain, spleen, lung, liver, skeleton muscle, kidney, testis, embryo day 7, 11, 15, and 17, placenta, eye, lymph node, smooth muscle, prostate, thymus, stomach, and uterus with PCR (Fig. 1). Selected PCR products were cloned and sequenced to confirm the exons and to reveal intron/exon junctions.

Transcript variants encoding functional Grx2 isoforms (*i.e.*, transcripts that encode all residues necessary for enzymatic activity and the Trx fold) consist of at least exons II, III, and IV. These transcripts were found to be expressed in all tissues. In addition, we identified a second ~120-bp larger product in testis (Fig. 1, second panel). Mitochondrial Grx2a (transcript variant 1, mGLRX2_v1), consisting of exons Ia, II, III, and IV, was detected in all tissues with the exception of testis, which is in agreement with earlier results (17) (Fig. 1, third panel). For the identification of an alternative splice-donor site within exon Ia implied by our EST analysis, we established a PCR that amplified both potential transcripts. We identified a truncated exon Ia^{trunc} that is 73 bp shorter than exon Ia. Because of this difference in size, we were able to distinguish between the two forms (Fig. 1, panel four). Subsequent sequencing confirmed the presence of this transcript variant (named mGLRX2_v2) in many tissues. Estimated from the density of the bands, an average of 80% of the mGLRX2_v1/mGLRX2_v2 transcripts contained exon Ia,

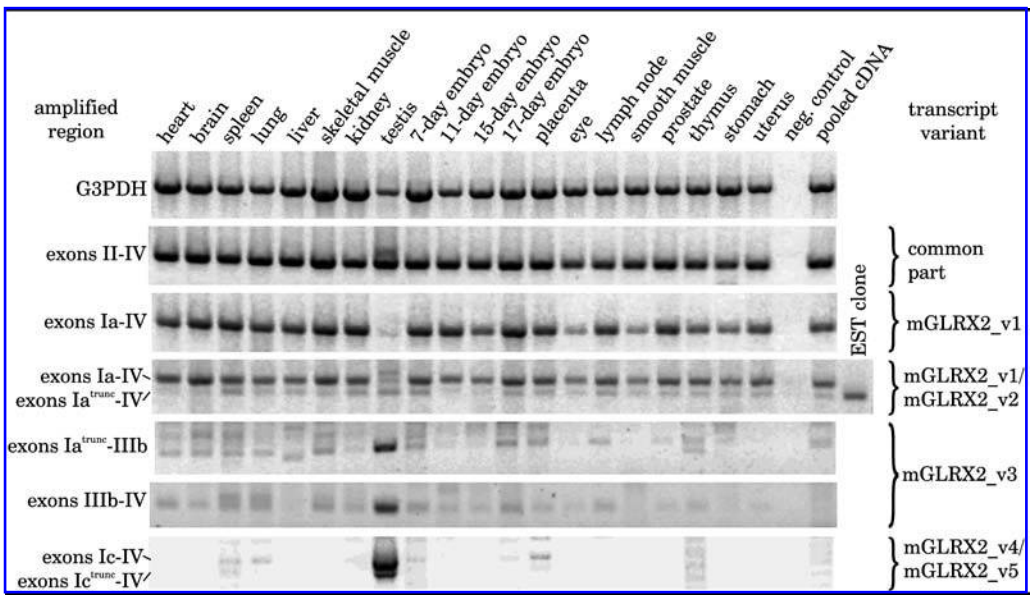

FIG. 1. RT-PCR analysis of the expression of different mGrx2 transcript variants in cDNA derived from different mouse tissues and pooled cDNA. Ten microliters of each PCR reaction was run on a 1.5% agarose gel (except Ia^{trunc}-IV = 2% agarose) containing 0.01% ethidium bromide in Tris-acetate-EDTA buffer. Negative control contained water as template, positive pooled cDNA. EST clone P998004867, used as positive control for transcript variant Ia^{trunc}-IV, was derived from the I.M.A.G.E. Consortium. A G3PDH oligonucleotide pair was used for cDNA integrity check in each tissue. Oligonucleotides and PCR conditions are summarized in Table I.

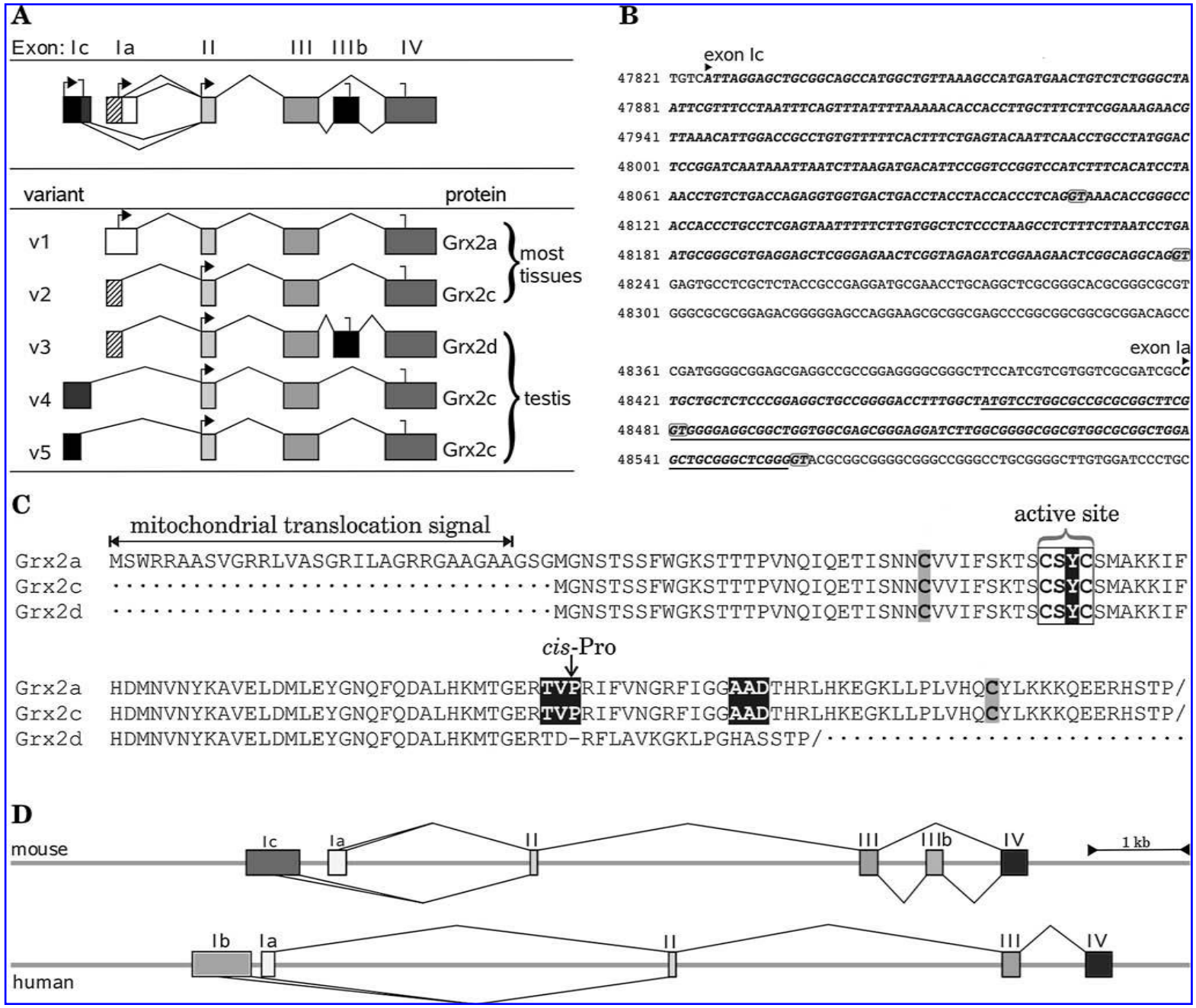
A
Exon: Ic Ia II III IIIb IV
variant
protein
v1
v2
v3
v4
v5
Grx2a
Grx2c
Grx2d
Grx2c
most tissues
testis
B
exon Ic
47821 TGTCATTAGGAGCTGCGGCAGCCATGGCTGTTAAAGCCATGATGAACTGTCTCTGGGCTA
47881 ATTCGTTTCCTAATTTCAGTTTATTTTAAAAACACCACCTTGCTTTCTTCGGAAAGAACG
47941 TTAAACATTGGACCGCCTGTGTTTTTCACTTTCTGAGTACAATTCAACCTGCCTATGGAC
48001 TCCGGATCAATAAATTAATCTTAAGATGACATTCCGGTCCGGTCCATCTTTCACATCCTA
48061 AACCTGTCTGACCAGAGGTGGTGACTGACCTACCTACCACCCTCAGGTAAACACCGGGCC
48121 ACCACCCTGCCTCGAGTAATTTTTCTTGTGGCTCTCCCTAAGCCTCTTTCTTAATCCTGA
48181 ATGCGGGCGTGAGGAGCTCGGGAGAACTCGGTAGAGATCGGAAGAACTCGGCAGGCAGGT
48241 GAGTGCCTCGCTCTACCGCCGAGGATGCGAACCTGCAGGCTCGCGGGCACGCGGGCGCGT
48301 GGGCGCGCGGAGACGGGGGAGCCAGGAAGCGCGGCGAGCCCGGCGGCGGCGCGGACAGCC
exon Ia
48361 CGATGGGGCGGAGCGAGGCCGCCGGAGGGGCGGGCTTCCATCGTCGTGGTCGCGATCGCC
48421 TGCTGCTCTCCCGGAGGCTGCCGGGGACCTTTGGCTATGTCCTGGCGCCGCGCGGCTTCG
48481 GTGGGGAGGCGGCTGGTGGCGAGCGGGAGGATCTTGGCGGGGCGGCGTGGCGCGGCTGGA
48541 GCTGCGGGCTCGGGGTACGCGGCGGGGCGGGCCGGGCCTGCGGGGCTTGTGGATCCCTGC
C
mitochondrial translocation signal
active site
Grx2a MSWRRAASVGRRLVASGRILAGRRGAAGAAGSGMGNSTSSFWGKSTTTPVNQIQETISNNCVVIFSKTSCSYCSMAKKIF
Grx2c ·····MGNSTSSFWGKSTTTPVNQIQETISNNCVVIFSKTSCSYCSMAKKIF
Grx2d ·····MGNSTSSFWGKSTTTPVNQIQETISNNCVVIFSKTSCSYCSMAKKIF
cis-Pro
Grx2a HDMNVNYKAVELDMLEYGNQFQDALHKMTGERTVPRIFVNGRFIGGAADTHRLHKEGKLLPLVHQCYLKKKQEERHSTP/
Grx2c HDMNVNYKAVELDMLEYGNQFQDALHKMTGERTVPRIFVNGRFIGGAADTHRLHKEGKLLPLVHQCYLKKKQEERHSTP/
Grx2d HDMNVNYKAVELDMLEYGNQFQDALHKMTGERTD-RFLAVKGKLPGHASSTP/·····
D
mouse
Ic Ia II III IIIb IV
1 kb
human
Ib Ia II III IV

FIG. 2.

TABLE 2. OVERVIEW OF GLRX2 EXONS AND TRANSCRIPT VARIANTS

Exons

Exon	*Size (coding region) Bp*	*Encodes*	*Splice acceptor*	*Splice donor*	*Intron*	*Intron size bp*
Ia	98	ATG, mitochondrial translocation signal	(-)	CGGGgtac	Ia-II	1889
Ia^{trunc}	0	(-)	(-)	TTCGgtgg	Ia^{trunc}-II	1963
Ic	0	(-)	(-)	GCAGgtga	Ic-II	2205
Ic^{trunc}	0	(-)	(-)	TCAGgtaa	Ic^{trunc}-II	2337
II	64	ATG, 1st nonactive site Cys	ttagAATG	CCAAgtga	II-III	3335
III	177	Active site, GSH binding	ttagGAAA	AACCgtga	III-IIIb	758
					III-IV	1284
IIIb	45	Alternative TGA	caagGACA	CAAGgtca	IIIb-IV	413
IV	132	*cis*-Pro, GSH binding, 2nd nonactive site Cys, TGA	acagGTTC	(-)	(-)	(-)

Transcript variants

Name	*Exons in mRNA*	*Open reading frame*	*Kozak sequence*[a]	*Encodes (protein isoform)*	*Amino acids*	*Expressed in (tissues)*
GLRX2_v1	Ia, II, III, IV	Ia-IV	T**CGG**GA**ATGG**	Grx2a (mitochondria)	156	All tissues, very low in testis
GLRX2_v2	Ia^{trunc}, II, III, IV	II-IV	CTTCGA**ATGG**	Grx2c (cytosol)	123	All tissues
GLRX2_v3	Ia^{trunc}, II, III, IIIb, IV	II-IIIb	CTTCGA**ATGG**	Grx2d (cytosol)	96	Testis
GLRX2_v4	Ic, II, III, IV	II-IV	**GGCA**GA**ATGG**	Grx2c (cytosol)	123	Testis
GLRX2_v5	Ic^{trunc}, II, III, IV	II-IV	CT**CA**GA**ATGG**	Grx2c (cytosol)	123	Testis

[a]Bold characters indicate consistencies with the general Kozak consensus sequence.

and 20%, Ia^{trunc}. Again, we obtained an additional larger product from testis cDNA. Sequencing of the larger products from the variant 2- and 3-specific PCR reactions as well as from the PCR specific for the common part of all variants (exons II–IV) revealed the third alternative transcript variant (mGLRX_v3). This variant consists of exons Ia^{trunc}, II, III, the newly identified single-cassette exon IIIb, and exon IV. We screened for variant mGLRX2_v3 amplifying fragments from both exons Ia^{trunc} to IIIb and exons IIIb to IV. The PCRs resulted in strong bands in testis samples, but only faint and inconsistent bands in independent samples derived from other tissues (Fig. 1, panels five and six).

As implied by the EST screening, we identified a new alternative first exon in the mouse GLRX2 gene. This exon is located upstream of exon Ia in a position similar to that of the human exon Ib; however, the sequences do not share significant homology. Our PCR screening for exon Ic resulted in the identification of transcript variants four and five. Because of two alternative splice donors in exon Ic, mGLRX2_v4 consists of exons Ic, II, III, and IV, mGLRX2_v5 contained a 132-bp shorter form of exon Ic, Ic^{trunc}, and exons II, III, and IV. Both forms are expressed predominantly in testis. The ratio between variants four and five in testis was found to be 2:1. By using 5′-RACE, we determined the transcription start point of mGLRX2_v4 and mGLRX2_v5 to be located 354 bp upstream of the splice-donor site of mGLRX2_v4 (Fig. 2B).

All experimentally verified mGLRX2 exons and transcript variants are summarized in Table 2 and Fig. 2. The five identified transcript variants encode three distinct proteins: (a) mGLRX2_v1 encodes the mitochondrial isoform Grx2a; (b) mGLRX2_v2, mGLRX2_v4, and mGLRX2_v5 share the same open reading frame and give rise to a protein entirely encoded by the constitutive exons II, III, and IV that is essentially identical to human cytosolic/nuclear Grx2c; and (c) mGLRX_v3 encodes the second new Grx2 isoform (named

FIG. 2. Summary of mouse GLRX2 transcript variants. (A) Alternative splicing of the mouse GLRX2 gene (*upper panel*) and transcript variants of mouse GLRX2 (*lower panel*). The longest possible open reading frames are indicated by *arrows* (start codons, translation initiation) and *hooks* (stop codons). (**B**) Sequence of exons Ic and Ia. The transcription start points are marked with *triangles*; the exons sequence are shown in *bold-italic* characters, experimentally determined splice donor sites are *boxed*, and the coding region of exon Ia is *underlined*. (**C**) Comparison of the primary structures of mouse Grx2a, Grx2c, and Grx2d. Some structurally and functionally important regions are indicated above the sequences. Residues important for GSH binding were printed on black, and the cysteines forming the structural disulfide on *gray* background. (**D**) Comparison of the human and mouse GLRX2 gene structures and alternative splicing/transcription initiation patterns. Note: With the exception of the 5′ of mouse exon Ic, homologous to a region immediately upstream of human exon Ib, mouse exon Ic and human exon Ib do not share significant sequence homology. The regions of highest homology are (in order of their degree of identity) exons III, exons Ia, exons IV, and exons II. Additional regions of high homology are centered in the middle of both introns II and III.

Grx2d) that is encoded by an open reading frame spanning from exon II to exon IIIb.

Properties of the mouse Grx2 protein isoforms

The newly identified cytosolic isoforms Grx2c and Grx2d were expressed in *E. coli* and purified for further characterization. Similar to the human counterpart (20), purified mouse Grx2c was not clear but appeared brownish. In gel-filtration chromatography, the protein (theoretic mass with 6-His tag, 16.5 kDa) separated into two fractions: a brownish dimeric fraction (apparent size, 36.4 kDa) and a clear monomeric fraction of 14.2 kDa (Fig. 3). The dimeric fraction exhibited the same spectral properties as human Grx2 (*i.e.*, two additional broad absorption bands at 320 and 428 nm) (Fig. 3). Similar to human Grx2, the monomeric fraction of mouse Grx2c was enzymatically active, with a specific activity of 11.3 ± 1.3 μmol/mg/min in the HED assay compared with 27.4 ± 2.3 μmol/mg/min for human Grx2c. To study a possible function of Grx2c in the cytosol, we tested the apoprotein for activity with mouse RNR. As shown in Fig. 4, Grx2c was able to donate electrons to RNR for the reduction of CDP, yielding a V_{max} of 0.43 nM dCDP/min ± 0.04. The k_m of RNR for Grx2 was determined to be 0.15 μM ± 0.05.

Unlike Grx2c, Grx2d was difficult to obtain, because it was not expressed as soluble protein in *E. coli*. This was not unexpected because the protein lacks some residues crucial for the thioredoxin fold, most notably the cis-proline residue (Fig. 2C). We purified Grx2d from inclusion bodies in the presence of guanidine hydrochloride and allowed the protein to refold in the presence of 500 m*M* NaCl and 50% glycerol at pH 8. According to CD spectroscopy, the *in vitro* folded protein exhibited a similar content of helices, sheets, and coiled regions as Grx2 (data not shown). However, the protein was inactive in the HED assay, even when assayed at high concentrations (*i.e.*, up to 0.5 μM).

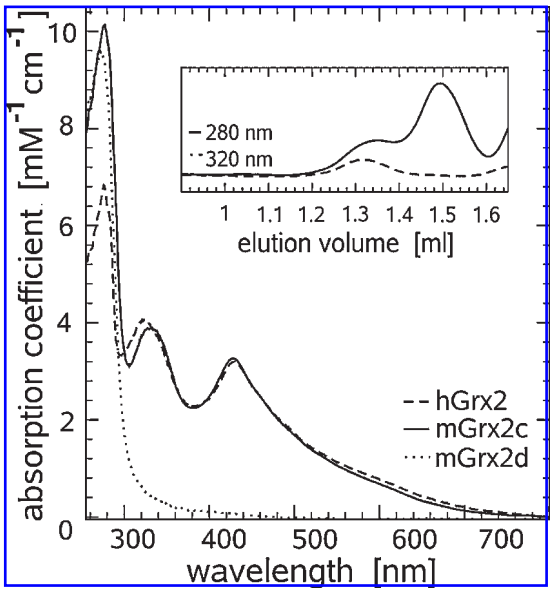

FIG. 3. FeS cluster binding to mouse Grx2. UV-visible absorption spectra of human Grx2 (*dashed line*), mouse Grx2c (*straight line*), and mouse Grx2d (*dotted line*). The spectral bands at 320 and 428 nm are in agreement with a 2Fe2S cluster, as demonstrated for human Grx2 before (20). *Inset*: Elution profile of mouse Grx2c purified on a Superdex 75 gel-filtration column at 280 nm (protein) and 320 nm ([Fe,S] chromophore). The determined molecular weights were 36.4 kDa for the colored dimeric protein and 14.2 kDa for the monomeric protein.

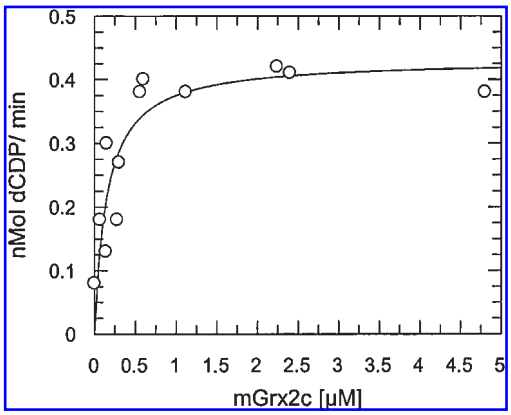

FIG. 4. Mouse Grx2c as electron donor for mouse ribonucleotide reductase. Michaelis–Menten plot of reaction velocity *versus* substrate concentration.

Immunologic detection of Grx2 in mouse tissues

First, we compared the reaction of mouse Grx2c and Grx2d with the antibodies obtained against human Grx2 in a specific sandwich ELISA (23). The standard curve for mouse Grx2c was colinear to the standard for human Grx2; however, the sensitivity was about sixfold lower. *In vitro* folded Grx2d did not react with the antibodies in a specific manner (Fig. 5A). Of course, this does not completely exclude that natively folded Grx2d may be recognized by the antibody. Next, we used ELISA to confirm and quantify the presence of Grx2 (*i.e.*, most likely the sum of Grx2a and Grx2c, in total extracts of different tissues) (Fig. 5B). Heart contained the highest amount of immunoreactive Grx2, followed by kidney, brain, testis, spleen, and liver. Because GLRX2_v1 (mitochondrial Grx2a) is basically absent from testis, these results provided further evidence for the presence of nonmitochondrial Grx2 in testis tissue.

Next, we studied the localization of Grx2 in mouse testis cell types with immunohistochemistry and confocal immunofluorescence microscopy in greater detail (Fig. 6). Grx2 immunolabeling resulted in a consistent and strong staining in spermatogonia that was concentrated in the cytoplasm (Fig. 6A and B). Interstitial Leydig cells showed some degree of staining, whereas all stages of spermatocytes and Sertoli cells showed only faint staining (Fig. 6A). Spermatids displayed the strongest Grx2 staining. Round spermatids showed a distinct cytosolic staining concentrated in one hemisphere of the cell (Fig. 6C and D). The 3D reconstruction of 62 layers within a 10-μm section revealed a concave, cuplike distribution of the protein (Fig. 6E). Staining of Grx2 in elongated spermatids resulted in an arrowhead-like structure on top of the elongated nuclei, pointing away from the lumen of the tubulus (Fig. 6F–H). The staining in both round and elongated spermatids is in agreement with acrosomal localization.

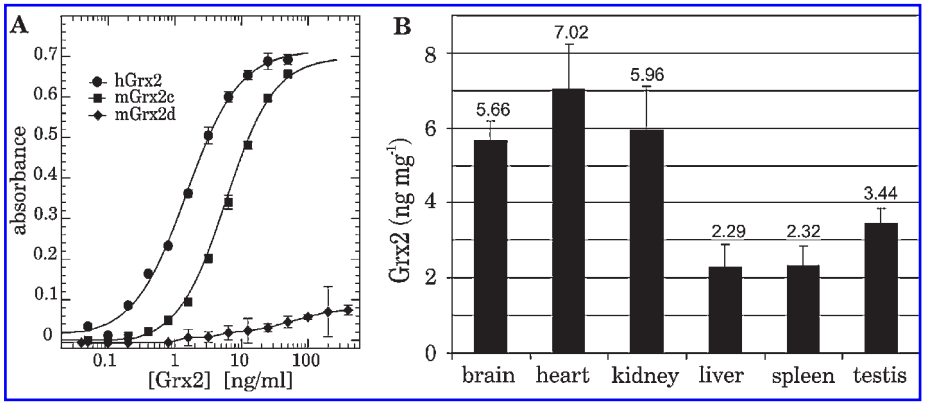

FIG. 5. Levels of Grx2 in tissues. (**A**) ELISA standard curves of human Grx2 (*circles*), mouse Grx2c (*squares*), and mouse Grx2d (*diamonds*) by using the sandwich ELISA described in (23). (**B**) Levels of Grx2 in mouse tissue by using mouse Grx2c as standard for quantification.

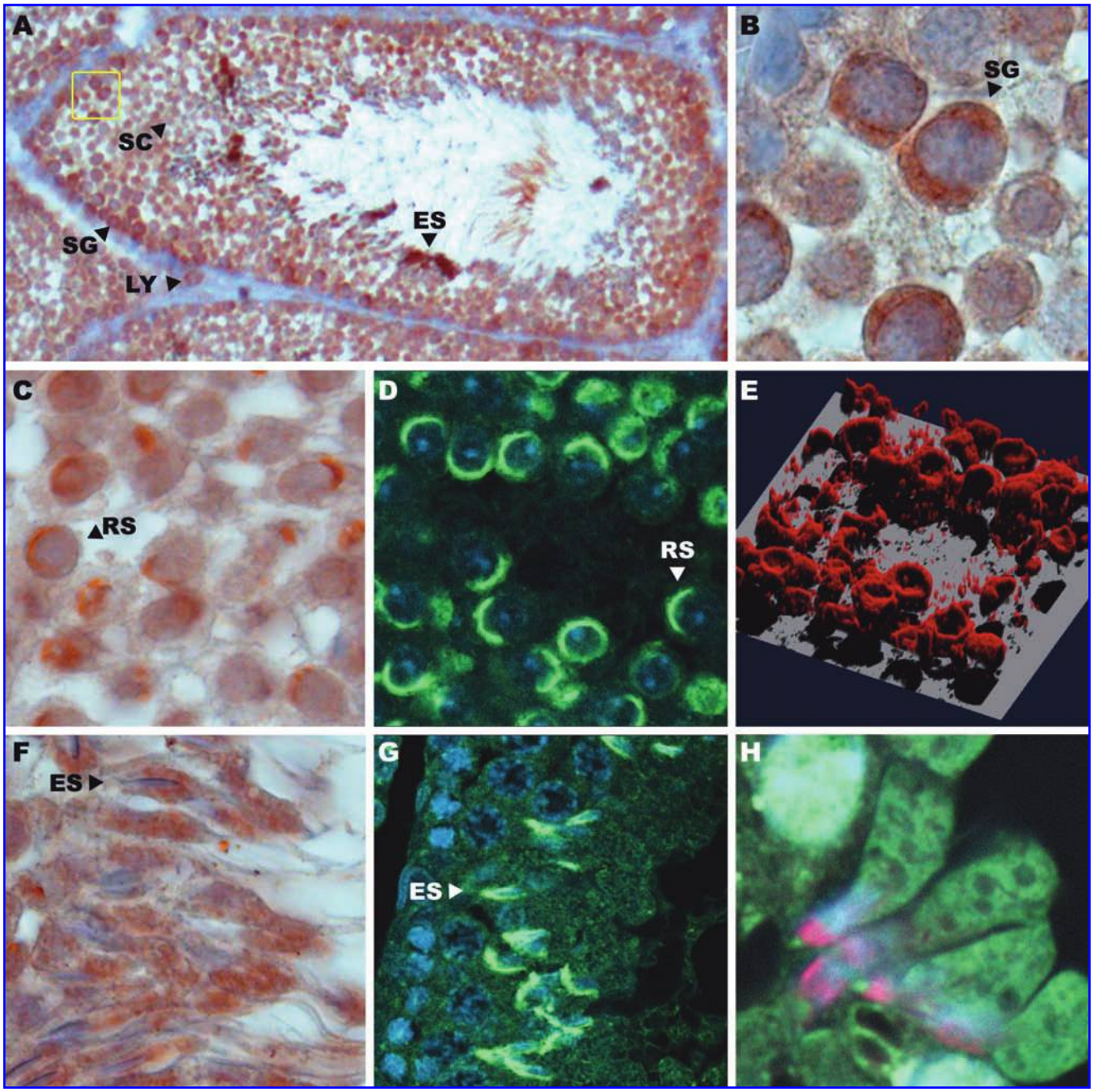

FIG. 6. Localization of Grx2 in mouse testis. (**A**) Light-microscopic localization of Grx2 revealed by staining with anti-mouse Grx2 antibodies. (**B**) Magnification of **A** (yellow frame) showing intense staining in the cytosol of spermatogonia (SG). (**C–E**) Staining of round spermatids (RSs). (**C**) Immunohistochemical staining of RS. (**D**) Confocal immunofluorescence detection of Grx2 in RS. (E) 3D-reconstruction of 62 layers of D spanning 10 μm. (**F–H**) Staining of elongated spermatids (ESs). (**F**) Immunohistochemical staining of ESs. (**G**) Confocal immunofluorescence detection of Grx2 in ESs. (**H**) Co-staining of Grx2 (red) with the cytosolic marker DNase I (green) and the nucleus (blue), analyzed with confocal microscopy. Further abbreviations: spermatocyte (SC) and Leydig cell (LY).

Further to investigate the presence of cytosolic Grx2 in cells, we developed a method for the co-staining of Grx2 with cytosolic (Dnase I for the staining of globular actin) and mitochondrial (anti-prohibitin 1 and anti-manganese superoxide dismutase) markers and analyzed the subcellular localization of Grx2 in different cells of the testis, the spleen, and the stomach, tissues that all exhibit a high amount of transcript encoding Grx2c (see Fig. 1). As expected, spermatogonia show a clear co-staining of Grx2 with the cytosolic (Fig. 7A) but not the mitochondrial marker (Fig. 7B). In stomach, parietal cells displayed mitochondrial co-staining with Grx2 (not shown). In enteroendocrine cells of the fundic glands, however, Grx2 does not co-stain with either of the mitochondrial marker proteins investigated (Fig. 7C and D). In spleen, cells of the red pulpa show a clear co-staining of Grx2 with mitochondria (Fig. 7E and F). In cells of the white pulpa, conversely, cells display mainly cytosolic localization of Grx2 (Fig. 7G and H). These results demonstrate the presence of cytosolic Grx2, presumably Grx2c, in specialized cells of different tissues, implying specific differences in Grx2 transcription and splicing in different cell types within a given tissue, at least in the three tissues investigated.

Discussion

Both the human and mouse GLRX2 genes are, by mechanisms of alternative transcription initiation and splicing, transcribed and processed into different mRNA variants that encode functionally different proteins. Alternative use of the genome is one of the striking differences between related species, and a number of similarities but also remarkable differences are noted between human and mouse Grx2 mRNA variants and protein isoforms (Fig. 2A and D).

The human GLRX2 gene consists of five exons: the constitutive exons II, III, and IV and the two alternative first exons Ia and Ib (22). Transcript variant 1 (hGLRX2_v1) is composed of exons Ia–IV and encodes Grx2a, hGLRX_v2 of exons Ib – IV (Grx2b), and alternative splicing of exon Ib yields hGLRX2_v3 (Grx2c). The ubiquitous Grx2a is a mitochondrial protein, and the testis-specific Grx2b and c are localized in both cytosol and nucleus. In the present study, we identified, confirmed, and characterized six exons in the mouse Grx2 gene (Fig. 2A). The three constitutive exons II, III, and IV, two alternatively transcribed first exons (exons Ia and Ic), which both contain two alternative splice-donor sites, and one single-cassette exon (exon IIIb), which resides between exons III and IV. These six exons give rise to five different transcript variants, which encode three different protein isoforms (see Fig. 2 and Table 2). From the six exons present in the mouse gene, only four (Ia, II, III, and IV) are conserved in the human counterpart. The human gene does not contain equivalents to mouse exons Ic and IIIb, and the mouse gene lacks a region homologous to human exon Ib. Humans and mice share the mitochondrial protein isoform Grx2a as well as the second major protein isoform, the cytosolic/nuclear Grx2c. Remarkably, Grx2c is expressed by different mechanisms in both species. In humans, it is derived from alternative splicing of exon Ib and therefore is restricted to testes (22). In mice, it is derived from alternative splicing of exons Ia and Ic. Cytosolic Grx2 is present in distinct cells of several mouse tissues, whereas neighboring cell types express primarily mitochondrial Grx2. Jurado *et al*. (17) analyzed the absolute gene-expression pattern of mouse Grx2 before. The number of mRNA molecules containing a fragment spanning from the 3′ end of exon I (Ia) to exon II corresponded to only 40% of the total number of Grx2 mRNA molecules. As the exon Ia primer binding site in (17) was located 3′ of the alternative splice donor site in exon Ia, we can conclude that at least part of the "missing" mRNA corresponded to mGLRX2_v2 encoding Grx2c.

This widely expressed cytosolic isoform of Grx2 in mouse was the most surprising finding of this study. What could be the function of a second Grx in the cytosol of some specific cells? Grx1 and Grx2 both catalyze the reduction of GSH-mixed disulfides with high specificity (16); however, *in vitro* Grx2 can be activated by oxidation, whereas the Grx1 activity is inhibited when the additional structural cysteine residues become oxidatively modified (10, 20). One might speculate that Grx2c serves as backup for Grx1 under certain conditions. Recently, two published studies described the effects of targeted disruption of the Grx1 gene in mice (11, 26). Surprisingly, lack of function of Grx1 was not lethal for mice, as described for Trx1 and Trx2 (29, 33). Moreover, the first study reported that loss of Grx1 did not sensitize adult mice to ischemia/reperfusion-induced injury or hypoxia, although embryonic fibroblasts were sensitized to oxidative stress (11). Somewhat controversy, the second study described that Grx1 deficiency depressed functional recovery and increased infarct size in coronary occlusion/reperfusion models of heart infarction and increased ROS production during ischemia and reperfusion (26). It is tempting to speculate that the mild phenotype described for the Grx1 knockout animals may be the result of complementation by transcriptional activation of Grx2c. In contrast to this hypothesis, Ho*et al*. (11) could not detect any compensatory deglutathionylation activity in different tissues of mice lacking Grx1. Of course, this does not exclude that cytosolic Grx2 may compensate for other important activities of Grx1 (for instance, the donation of electrons to RNR). It will be interesting to see the expression and distribution of cytosolic Grx2 in these animals.

Our results confirm earlier observations (17) that mice testes lack significant amounts of mGLRX2_v1 encoding Grx2a. Instead, our data demonstrate the transcription of

FIG. 7. Immunological detection of cytosolic Grx2 in cells of the testis, the stomach, and the spleen with confocal microscopy. Co-staining with the cytosolic maker DNase I that stains globular actin, and the two mitochondrial marker proteins prohibitin 1 and manganese superoxide dismutase (Mn-SOD) was described in detail in the experimental procedures section. (**A,B**) Co-staining of Grx2 in spermatogonia with DNase I (**A**) but not mitochondrial prohibitin 1 (**B**). (**C, D**) In enteroendocrine cells of the fundic gland in stomach, Grx2 colocalizes with neither mitochondrial Mn-SOD (**C**) nor with prohibitin 1 (**D**). (**E, F**) Cells of the red pulpa of the spleen lack co-staining of Grx2 with DNase I (**E**), but show a high degree of colocalization with mitochondrial prohibitin 1 (**F**). (**G, H**) Cells of the white pulpa of spleen, conversely, show a high degree of overlap with the cytosolic marker (**G**), but only a small degree of overlap with the mitochondrial marker (**H**).

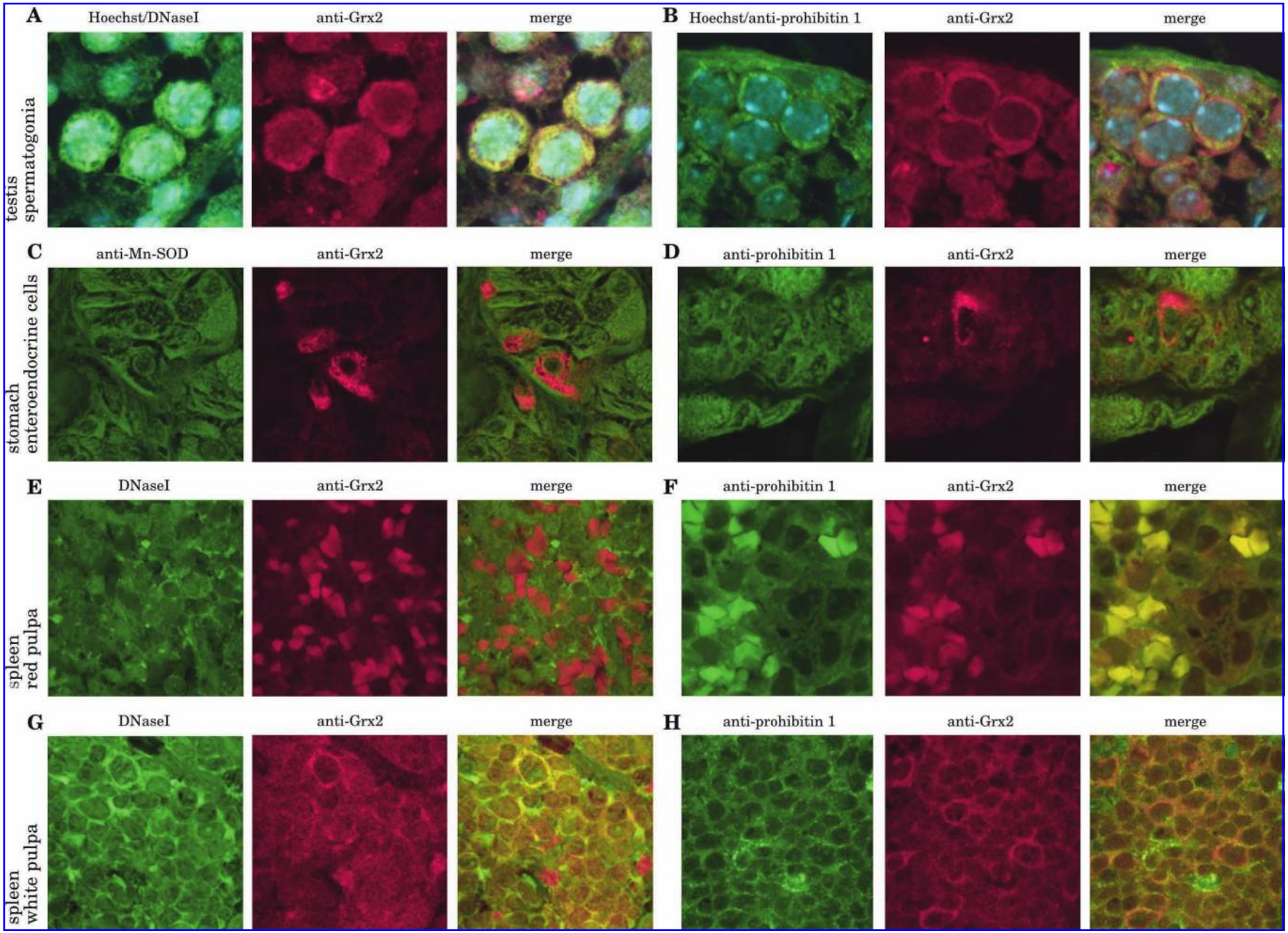
A
Hoechst/DNaseI
anti-Grx2
merge
B
Hoechst/anti-prohibitin 1
anti-Grx2
merge
testis
spermatogonia
C
anti-Mn-SOD
anti-Grx2
merge
D
anti-prohibitin 1
anti-Grx2
merge
stomach
enteroendocrine cells
E
DNaseI
anti-Grx2
merge
F
anti-prohibitin 1
anti-Grx2
merge
spleen
red pulpa
G
DNaseI
anti-Grx2
merge
H
anti-prohibitin 1
anti-Grx2
merge
spleen
white pulpa

FIG. 7.

three additional mRNA variants, mGLRX2_v3, v4, and v5 encoding Grx2d and Grx2c, respectively, in testis. Immunohistochemical staining of Grx2 in the cytosol of spermatogonia provides evidence for the presence of Grx2c in these cells. The transcript of variant 3 demonstrated by both RT-PCR and 5′RACE is the only evidence so far for the putative protein isoform Grx2d. It may be worth mentioning that exon IIIb appears to be unique to mice. It is absent from human and contains five nucleotide deletions over three different parts in the rat genome. We can estimate from the relative intensities of the bands shown in Fig. 1 that v4 (Grx2c) accounts for ~50%, and both v3 (Grx2d) and v5 (Grx2c), for about 25% of the total Grx2 mRNA in testicular tissue. What could be the function of additional Grx2 isoforms in testis? Spermatogenesis is a highly complex process of cellular differentiation that takes place in the seminiferous tubules of the testis. The male germ cell differentiation starts with the proliferation of diploid germ cells (spermatogonia) followed by meiotic division of spermatocytes, and finally, differentiation of haploid spermatides into sperm. Cell division and DNA synthesis require a constant supply of deoxyribonucleotides by RNR. Surprisingly, neither of the established electron donors for RNR (Trx1 and Grx1) colocalizes with the enzyme in rat and calf testes. RNR is localized primarily in spermatogonia (9, 36); Trx1 was found to be highly expressed in the interstitial Leydig cells and a small fraction of spermatogonia (9, 37). Prominent staining of Grx1 was detected in Sertoli cells, and weak staining, in Leydig cells. We showed that Grx2c can serve as electron donor for RNR in sub-micromolar concentrations (*i.e.*, physiologic concentrations). Thus, cytosolic Grx2 is the only confirmed electron donor for RNR that colocalizes with the enzyme in spermatogonia.

During maturation of spermatids and sperm, oxidative crosslinking of proteins through specific disulfide linkages leads to the formation of structural sperm components (42, 47). A number of members of the Trx family of proteins take part in these events: spermatocyte/spermatid-specific thioredoxin 1 and 2, which both contain a Trx domain as part of a larger protein, are found in the fibrous sheet of the sperm (31, 39); spermatocyte/spermatid-specific thioredoxin 3 is associated with the Golgi apparatus of spermatids (14); and thioredoxin like 2 is associated with microtubuli in cilia and flagella (40). TGR staining was detected in elongating spermatids and associated with the vicinities of the assembling mitochondrial sheath (44). Similar to Grx2, the phospholipid hydroperoxide reductase (PHGPx) gene gives rise to two testis-specific isoforms targeted to mitochondria and the nucleus, respectively (18, 34, 35, 41). PHGPx is present in soluble form in early spermatids but persists in mature sperm as a structural component of the mitochondrial midpiece capsule (48). The apparent colocalization of Grx2 with acrosomal structures in both round and elongated spermatids suggests a similar structural function of the protein or a role in the formation of these disulfides.

In conclusion, we detected and characterized two new Grx2 protein isoforms in mice: cytosolic Grx2c, which can complex with a 2Fe2S cluster and serve as electron donor for RNR, and a testis-specific variant, Grx2d, of unknown function. These results suggest additional specific functions of Grx2 in multiple tissues of mice.

Acknowledgments

Christoph Hudemann and Maria Elisabet Lönn contributed equally to this work. We thank Drs. Elias Arnér and Hans-Peter Elsässer for helpful discussions, Waltraud Ackermann and Sabrina Oesteritz for excellent technical assistance. and Karin Beimborn, Gisela Lesch. and Lena Ringdén for excellent administrative assistance. This work was supported by grants from the Deutsche Forschungsgemeinschaft (SFB593-N01), Karolinska Institutet, the Swedish Cancer Society, and the Swedish Society for Medical Research. F.Z.A. was supported by a fellowship by the ministry of Health I.R. Iran.

Abbreviations

ELISA, enzyme-linked immunosorbent assay; EST, expressed sequence tag; G3PDH, glyceralaldehyde-3-phosphate dehydrogenase; Grx, glutaredoxin; GSH, glutathione (reduced); GSSG, glutathione disulfide; HED, hydroxyethyl disulfide; Mn-SOD, manganese superoxide dismutase; RNR, ribonucleotide reductase; ROS, reactive oxygen species; RT-PCR, reverse transcription polymerase chain reaction; TGR, thioredoxin glutathione reductase; Trx, thioredoxin; TrxR, thioredoxin reductase; UTR, untranslated region.

References

1. Altschul SF, Gish W, Miller W, Meyers EW, and Lipman DJ. Basic local alignment search tool. *J Mol Biol* 215: 403–410, 1990.
2. Beer SM, Taylor ER, Brown SE, Dahm CC, Costa NJ, Runswick MJ, and Murphy MP. Glutaredoxin 2 catalyses the reversible oxidation and glutathionylation of mitochondrial membrane thiol proteins. *J Biol Chem* 279: 47939–47951, 2004.
3. Berndt C, Hudemann C, Hanschmann EM, Axelsson R, Holmgren A, and Lillig CH. How does iron-sulfur cluster coordination regulate the activity of human glutaredoxin 2? *Antioxid Redox Signal* 9: 151–157, 2007.
4. Berndt C, Lillig CH, and Holmgren A. Thiol-based mechanisms of the thioredoxin and glutaredoxin systems: implications for diseases in the cardiovascular system. *Am J Physiol Heart Circ Physiol* 292: 1227–1236, 2007.
5. Chrestensen CA, Starke DW, and Mieyal JJ. Acute cadmium exposure inactivates thioltransferase (glutaredoxin), inhibits intracellular reduction of protein-glutathionyl-mixed disulfides, and initiates apoptosis. *J Biol Chem* 275: 26556–26565, 2000.
6. Davis R, Thelander M, Mann GJ, Behravan G, Soucy F, Beaulieu P, Lavallee P, Graslund A, and Thelander L. Purification, characterization, and localization of subunit interaction area of recombinant mouse ribonucleotide reductase R1 subunit. *J Biol Chem* 269: 23171–23176, 1994.
7. Enoksson M, Fernandes AP, Prast S, Lillig CH, Holmgren A, and Orrenius S. Overexpression of glutaredoxin 2 attenuates apoptosis by preventing cytochrome c release. *Biochem Biophys Res Commun* 327: 774–779, 2005.
8. Gladyshev VN, Liu A, Novoselov SV, Krysan K, Sun QA, Kryukov VM, Kryukov GV, and Lou MF. Identification and characterization of a new mammalian glutaredoxin (thioltransferase), Grx2. *J Biol Chem* 276: 30374–30380, 2001.
9. Hansson HA, Rozell B, Stemme S, Engstrîm Y, Thelander L, and Holmgren A. Different cellular distribution of thioredoxin and subunit M1 of ribonucleotide reductase in rat tissues. *Exp Cell Res* 163: 363–369, 1986.

10. Hashemy SI, Johansson C, Berndt C, Lillig CH, and Holmgren A. Oxidation and S-nitrosylation of cysteines in human cytosolic and mitochondrial glutaredoxins: effects on structure and activity. *J Biol Chem* 282:14428–14436, 2007.
11. Ho YS, Xiong Y, Ho DS, Gao J, Chua BH, Pai H, and Mieyal JJ. Targeted disruption of the glutaredoxin 1 gene does not sensitize adult mice to tissue injury induced by ischemia/reperfusion and hyperoxia. *Free Radic Biol Med* 43: 1299–1312, 2007.
12. Holmgren A. Hydrogen donor system for Escherichia coli ribonucleoside-diphosphate reductase dependent upon glutathione. *Proc Natl Acad Sci U S A* 73: 2275–2279, 1976.
13. Holmgren A. Thioredoxin and glutaredoxin systems. *J Biol Chem* 264: 13963–13966, 1989.
14. Jimenez A, Zu W, Rawe VY, Pelto-Huikko M, Flickinger CJ, Sutovsky P, Gustafsson JA, Oko R, and Miranda-Vizuete A. Spermatocyte/spermatid-specific thioredoxin-3, a novel Golgi apparatus-associated thioredoxin, is a specific marker of aberrant spermatogenesis. *J Biol Chem* 279: 34971–34978, 2004.
15. Johansson C, Kavanagh KL, Gileadi O, and Oppermann U. Reversible sequestration of active site cysteines in a 2FE2S-bridged dimer provides a mechanism for glutaredoxin 2 regulation in human mitochondria. *J Biol Chem* 282: 3077–3082, 2007.
16. Johansson C, Lillig CH, and Holmgren A. Human mitochondrial glutaredoxin reduces S-glutathionylated proteins with high affinity accepting electrons from either glutathione or thioredoxin reductase. *J Biol Chem* 279: 7537–7543, 2004.
17. Jurado J, Prieto-Alamo MJ, Madrid-Risquez J, and Pueyo C. Absolute gene expression patterns of thioredoxin and glutaredoxin redox systems in mouse. *J Biol Chem* 278: 45546–45554, 2003.
18. Kelner MJ and Montoya MA. Structural organization of the human selenium-dependent phospholipid hydroperoxide glutathione peroxidase gene (GPX4): chromosomal localization to 19p133. *Biochem Biophys Res Commun* 249: 53–55, 1998.
19. Lillig CH and Holmgren A. Thioredoxin and related molecules: from biology to health and disease. *Antioxid Redox Signal* 9: 25–47, 2007.
20. Lillig CH, Berndt C, Vergnolle O, Lönn ME, Hudemann C, Bill E, and Holmgren A. Characterization of human glutaredoxin 2 as iron-sulfur protein: a possible role as redox sensor. *Proc Natl Acad Sci U S A* 102: 8168–8173, 2005.
21. Lillig CH, Lönn ME, Enoksson M, Fernandes AP, and Holmgren A. Short interfering RNA-mediated silencing of glutaredoxin 2 increases the sensitivity of HeLa cells towards doxorubicin and phenylarsine oxide. *Proc Natl Acad Sci U S A* 101: 13227–13232, 2004.
22. Lönn ME, Hudemann C, Berndt C, Cherkasov V, Capani F, Holmgren A, and Lillig CH. Expression pattern of human glutaredoxin 2 isoforms: identification and characterization of two testis/cancer cell-specific isoforms. *Antioxid Redox Signal* 10: 547–558, 2008.
23. Lundberg M, Fernandes AP, Kumar S, and Holmgren A. Cellular and plasma levels of human glutaredoxin 1 and 2 detected by sensitive ELISA systems. *Biochem Biophys Res Commun* 319: 801–809, 2004.
24. Lundberg M, Johansson C, Chandra J, Enoksson M, Jacobsson G, Ljung J, Johansson M, and Holmgren A. Cloning and expression of a novel human glutaredoxin (GRX2) with mitochondrial and nuclear isoforms. *J Biol Chem* 276: 26269–26275, 2001.
25. Luthman *M* and Holmgren A. Glutaredoxin from calf thymus purification to homogeneity. *J Biol Chem* 257: 6686–6689, 1982.
26. Malik G, Nagy N, Ho YS, Maulik N, and Das DK. Role of glutaredoxin-1 in cardioprotection: an insight with Glrx1 transgenic and knockout animals. *J Mol Cell Cardiol* 44: 261–269, 2008.
27. Mann GJ, Graslund A, Ochiai E, Ingemarson R, and Thelander L. Purification and characterization of recombinant mouse and herpes simplex virus ribonucleotide reductase R2 subunit. *Biochemistry* 30: 1939–1947, 1991.
28. Martin JL. Thioredoxin: a fold for all reasons. *Structure* 3: 245–250, 1995.
29. Matsui M, Oshima M, Oshima H, Takaku K, Maruyama T, Yodoi J, and Taketo MM. Early embryonic lethality caused by targeted disruption of the mouse thioredoxin gene. *Dev Biol* 178: 179–185, 1996.
30. Miranda-Vizuete A, Damdimopoulos AE, and Spyrou G. The mitochondrial thioredoxin system. *Antioxid Redox Signal* 101: 13227–13232, 2000.
31. Miranda-Vizuete A, Ljung J, Damdimopoulos AE, Gustafsson JA, Oko R, Pelto-Huikko M, and Spyrou G. Characterization of Sptrx, a novel member of the thioredoxin family specifically expressed in human spermatozoa. *J Biol Chem* 276: 31567–31574, 2001.
32. Murata H, Ihara Y, Nakamura H, Yodoi J, Sumikawa K, and Kondo T. Glutaredoxin exerts an antiapoptotic effect by regulating the redox state of Akt. *J Biol Chem* 278: 50226–50233, 2003.
33. Nonn L, Williams RR, Erickson RP, and Powis G. The absence of mitochondrial thioredoxin 2 causes massive apoptosis, exencephaly, and early embryonic lethality in homozygous mice. *Mol Cell Biol* 23: 916–922, 2003.
34. Pfeifer H, Conrad M, Roethlein D, Kyriakopouluos A, Brielmeier M, Bornkamm GW, and Behne D. Identification of a specific sperm nuclei selenoenzyme necessary for protamine thiol cross-linking during sperm maturation. *FASEB J* 15: 1236–1238, 2001.
35. Roveri A, Maiorino M, Nissi C, and Ursini F. Purification and characterization of phospholipid hydroperoxide glutathione peroxidase from rat testis mitochondrial membranes. *Biochim Biophys Acta* 1208: 211–221, 1994.
36. Rozell B, Barcena JA, Martinez-Galisteo E, Padilla CA, and Holmgren A. Immunochemical characterization and tissue distribution of glutaredoxin (thioltransferase) from calf. *Eur J Cell Biol* 62: 314–323, 1993.
37. Rozell B, Hansson HA, Luthman M, and Holmgren A. Immunohistochemical localization of thioredoxin and thioredoxin reductase in adult rats. *Eur J Cell Biol* 38: 79–86, 1985.
38. Rudolph R and Lilie H. In vitro folding of inclusion body proteins. *FASEB J* 10: 49–56, 1996.
39. Sadek CM, Damdimopoulos AE, Pelto-Huikko M, Gustafsson JA, Spyrou G, and Miranda-Vizuete A. Sptrx-2, a fusion protein composed of one thioredoxin and three tandemly repeated NDP-kinase domains is expressed in human testis germ cells. *Genes Cells* 6: 1077–1091, 2001.
40. Sadek CM, Jimenez, A, Damdimopoulos AE, Kieselbach T, Nord M, Gustafsson JA, Spyrou G, Davies EC, Oko R, van der Hoorn FA, and Miranda-Vizuete A. Characterization of human thioredoxin-like 2 A novel microtubule-binding thioredoxin expressed predominantly in the cilia of lung airway epithelium and spermatid manchette and exoneme. *J Biol Chem* 278: 13133–13142, 2003.
41. Schneider M, Vogt Weisenhorn DM, Seiler A, Bornkamm GW, Brielmeier M, and Conrad M. Embryonic expression

profile of phospholipid hydroperoxide glutathione peroxidase. *Gene Expr Patterns* 6: 489–494, 2006.
42. Shalgi R, Seligman J, and Kosower NS. Dynamics of the thiol status of rat spermatozoa during maturation: analysis with the fluorescent labeling agent monobromobimane. *Biol Reprod* 40: 1037–1045, 1989.
43. Shelton MD, Chock PB, and Mieyal JJ. Glutaredoxin: role in reversible protein S-glutathionylation and regulation of redox signal transduction and protein translocation. *Antioxid Redox Signal* 7: 348–366, 2005.
44. Su D, Novoselov SV, Sun QA, Moustafa ME, Zhou Y, Oko R, Hatfield DL, and Gladyshev VN. Mammalian selenoprotein thioredoxin-glutathione reductase: roles in disulfide bond formation and sperm maturation. *J Biol Chem* 280: 26491–26498, 2005.
45. Sun C, Berardi MJ, and Bushweller JH. The NMR solution structure of human glutaredoxin in the fully reduced form. *J Mol Biol* 280: 687–701, 1998.
46. Sun QA, Kirnarskydagger L, Shermandagger S, and Gladyshev VN. Selenoprotein oxidoreductase with specificity for thioredoxin and glutathione systems. *Proc Natl Acad Sci U S A* 98: 3673–3678, 2001.
47. Sutovsky P, Tengowski MW, Navara CS, Zoran SS, and Schatten G. Mitochondrial sheath movement and detachment in mammalian, but not nonmammalian, sperm induced by disulfide bond reduction. *Mol Reprod Dev* 47: 79–86, 1997.
48. Ursini F, Heim S, Kiess M, Maiorino M, Roveri A, Wissling J, and Flohe L. Dual function of the selenoprotein PHGPx during sperm maturation. *Science* 285: 1393–1396, 1999.
49. Wang J, Boja ES, Tan W, Tekle E, Fales HM, English S, Mieyal JJ, and Chock PB. Reversible glutathionylation regulates actin polymerization in A431 cells. *J Biol Chem* 276: 47763–47766, 2001.
50. Wells WW, Xu DP, Yang YF, and Rocque PA. Mammalian thioltransferase (glutaredoxin) and protein disulfide isomerase have dehydroascorbate reductase activity. *J Biol Chem* 265: 15361–15364, 1990.

Address reprint requests to:
Christopher Horst Lillig
Institute for Clinical Cytobiology and Cytopathology
Phillips UniversitÑt
DE-35037 Marburg, Germany

E-mail: horst@lillig.de

Date of first submission to ARS Central, March 5, 2008; date of final revised submission, June 24, 2008; date of acceptance, June 24, 2008.

This article has been cited by:

1. Jeong-Tae Yeon, Sik-Won Choi, Kie-In Park, Min-Kyu Choi, Jeong-Joong Kim, Byung-Soo Youn, Myeung-Su Lee, Jae-Min Oh. 2012. Glutaredoxin2 isoform b (Glrx2b) promotes RANKL-induced osteoclastogenesis through activation of the p38-MAPK signaling pathway. *BMB reports* **45**:3, 171-176. [CrossRef]
2. Elias S.J. Arnér . 2011. Redox Pioneer: Professor Arne Holmgren. *Antioxidants & Redox Signaling* **15**:3, 845-851. [Abstract] [Full Text HTML] [Full Text PDF] [Full Text PDF with Links] [Supplemental material]
3. Ying Xiong , Joachim D. Uys , Kenneth D. Tew , Danyelle M. Townsend . 2011. S-Glutathionylation: From Molecular Mechanisms to Health Outcomes. *Antioxidants & Redox Signaling* **15**:1, 233-270. [Abstract] [Full Text HTML] [Full Text PDF] [Full Text PDF with Links]
4. José R. Godoy, Sabrina Oesteritz, Eva-Maria Hanschmann, Wymke Ockenga, Waltraud Ackermann, Christopher Horst Lillig. 2011. Segment-specific overexpression of redoxins after renal ischemia and reperfusion: protective roles of glutaredoxin 2, peroxiredoxin 3, and peroxiredoxin 6. *Free Radical Biology and Medicine* **51**:2, 552-561. [CrossRef]
5. M. H. Visagie, A. M. Joubert. 2011. 2-Methoxyestradiol-bis-sulfamate induces apoptosis and autophagy in a tumorigenic breast epithelial cell line. *Molecular and Cellular Biochemistry* . [CrossRef]
6. Ricardo A. Azevedo, Rogério F. Carvalho, Mariana C. Cia, Priscila L. Gratão. 2011. Sugarcane Under Pressure: An Overview of Biochemical and Physiological Studies of Abiotic Stress. *Tropical Plant Biology* **4**:1, 42-51. [CrossRef]
7. Maria Laura Aon-Bertolino, Juan Ignacio Romero, Pablo Galeano, Mariana Holubiec, Maria Sol Badorrey, Gustavo Ezequiel Saraceno, Eva-Maria Hanschmann, Christopher Horst Lillig, Francisco Capani. 2011. Thioredoxin and glutaredoxin system proteins—immunolocalization in the rat central nervous system. *Biochimica et Biophysica Acta (BBA) - General Subjects* **1810**:1, 93-110. [CrossRef]
8. L. R. Fischer, A. Igoudjil, J. Magrane, Y. Li, J. M. Hansen, G. Manfredi, J. D. Glass. 2011. SOD1 targeted to the mitochondrial intermembrane space prevents motor neuropathy in the Sod1 knockout mouse. *Brain* **134**:1, 196-209. [CrossRef]
9. A. Ferri, P. Fiorenzo, M. Nencini, M. Cozzolino, M. G. Pesaresi, C. Valle, S. Sepe, S. Moreno, M. T. Carri. 2010. Glutaredoxin 2 prevents aggregation of mutant SOD1 in mitochondria and abolishes its toxicity. *Human Molecular Genetics* **19**:22, 4529-4542. [CrossRef]
10. Mohammad Moshahid Khan, Md. Nasrul Hoda, Tauheed Ishrat, Ajmal Ahmad, Mohammad Badruzzaman Khan, Gulrana Khuwaja, Syed Shadab Raza, Mohammed M. Safhi, Fakhrul Islam. 2010. Amelioration of 1-methyl-4-phenyl-1,2,3,6-tetrahydropyridine-induced behavioural dysfunction and oxidative stress by Pycnogenol in mouse model of Parkinson#s disease. *Behavioural Pharmacology* **21**:5-6, 563-571. [CrossRef]
11. Salman Azhar. 2010. Peroxisome proliferator-activated receptors, metabolic syndrome and cardiovascular disease. *Future Cardiology* **6**:5, 657-691. [CrossRef]
12. H-H Wu, Y-W Cheng, J T Chang, T-C Wu, W-S Liu, C-Y Chen, H Lee. 2010. Subcellular localization of apurinic endonuclease 1 promotes lung tumor aggressiveness via NF-#B activation. *Oncogene* **29**:30, 4330-4340. [CrossRef]
13. Kevin G. Hoff, Stephanie J. Culler, Peter Q. Nguyen, Ryan M. McGuire, Jonathan J. Silberg, Christina D. Smolke. 2009. In Vivo Fluorescent Detection of Fe-S Clusters Coordinated by Human GRX2. *Chemistry & Biology* **16**:12, 1299-1308. [CrossRef]
14. Md. Kaimul Ahsan , Istvan Lekli , Diptarka Ray , Junji Yodoi , Dipak K. Das . 2009. Redox Regulation of Cell Survival by the Thioredoxin Superfamily: An Implication of Redox Gene Therapy in the Heart. *Antioxidants & Redox Signaling* **11**:11, 2741-2758. [Abstract] [Full Text HTML] [Full Text PDF] [Full Text PDF with Links]
15. Andrea Henriques-Pons, Kanneboyina Nagaraju. 2009. Nonimmune mechanisms of muscle damage in myositis: role of the endoplasmic reticulum stress response and autophagy in the disease pathogenesis. *Current Opinion in Rheumatology* **21**:6, 581-587. [CrossRef]
16. Elena Andreucci, Benedetta Bianchi, Ilaria Carboni, Giancarlo Lavoratti, Marzia Mortilla, Claudio Fonda, Minna Bigozzi, Maurizio Genuardi, Sabrina Giglio, Ivana Pela. 2009. Inner ear abnormalities in four patients with dRTA and SNHL: clinical and genetic heterogeneity. *Pediatric Nephrology* **24**:11, 2147-2153. [CrossRef]
17. L. Wobbe, O. Blifernez, C. Schwarz, J. H. Mussgnug, J. Nickelsen, O. Kruse. 2009. Cysteine modification of a specific repressor protein controls the translational status of nucleus-encoded LHCII mRNAs in Chlamydomonas. *Proceedings of the National Academy of Sciences* **106**:32, 13290-13295. [CrossRef]
18. Janina Hamberger, Manuel Liebeke, Maria Kaiser, Karin Bracht, Ulrike Olszewski, Robert Zeillinger, Gerhard Hamilton, Dagmar Braun, Patrick J. Bednarski. 2009. Characterization of chemosensitivity and resistance of human cancer cell lines to platinum(II) versus platinum(IV) anticancer agents. *Anti-Cancer Drugs* **20**:7, 559-572. [CrossRef]

19. Makoto Naoi, Wakako Maruyama. 2009. Functional mechanism of neuroprotection by inhibitors of type B monoamine oxidase in Parkinson's disease. *Expert Review of Neurotherapeutics* **9**:8, 1233-1250. [CrossRef]
20. E ARNER. 2009. Focus on mammalian thioredoxin reductases — Important selenoproteins with versatile functions. *Biochimica et Biophysica Acta (BBA) - General Subjects* **1790**:6, 495-526. [CrossRef]
21. Molly M. Gallogly , David W. Starke , John J. Mieyal . 2009. Mechanistic and Kinetic Details of Catalysis of Thiol-Disulfide Exchange by Glutaredoxins and Potential Mechanisms of Regulation. *Antioxidants & Redox Signaling* **11**:5, 1059-1081. [Abstract] [Full Text PDF] [Full Text PDF with Links]
22. Louis Hermo, R.-Marc Pelletier, Daniel G. Cyr, Charles E. Smith, R.-Marc Pelletier. 2009. Surfing the wave, cycle, life history, and genes/proteins expressed by testicular germ cells. Part 5: Intercellular junctions and contacts between germs cells and Sertoli cells and their regulatory interactions, testicular cholesterol, and genes/proteins associated with more than one germ cell generation. *Microscopy Research and Technique* NA-NA. [CrossRef]
23. Xing-Huang Gao, Mariette Bedhomme, Laure Michelet, Mirko Zaffagnini, Stéphane D. LemaireChapter 12 Glutathionylation in Photosynthetic Organisms **52**, 363-403. [CrossRef]